

A deep *Chandra* observation of the Centaurus cluster: bubbles, filaments and edges

A.C. Fabian^{1*}, J.S. Sanders¹, G.B Taylor^{2,3} and S.W. Allen^{1,2}

¹ *Institute of Astronomy, Madingley Road, Cambridge CB3 0HA*

² *Kavli Institute for Particle Astrophysics and Cosmology, Stanford University, 382 Via Pueblo Mall, Stanford, CA 94305-4060, USA*

³ *National Radio Astronomy Observatory, Socorro, NM 87801, USA*

21 November 2018

ABSTRACT

X-ray images and gas temperatures taken from a deep ~ 200 ks *Chandra* observation of the Centaurus cluster are presented. Multiple inner bubbles and outer semicircular edges are revealed, together with wispy filaments of soft X-ray emitting gas. The frothy central structure and eastern edge are likely due to the central radio source blowing bubbles in the intracluster gas. The semicircular edges to the surface brightness maps 32 kpc to the east and 17.5 kpc to the west are marked by sharp temperature increases and abundance drops. The edges could be due to sloshing motions of the central potential, or are possibly enhanced by earlier radio activity. The high abundance of the innermost gas (about 2.5 times Solar) limits the amount of diffusion and mixing taking place.

Key words: X-rays: galaxies — galaxies: clusters: individual: Centaurus — intergalactic medium

1 INTRODUCTION

The Centaurus cluster (Abell 3526) is X-ray bright, being the nearest cluster (redshift $z = 0.0104$) with a 2–10 keV luminosity exceeding 5×10^{43} erg s⁻¹. Our earlier 31.7 ks *Chandra* image of the Centaurus cluster revealed a complex structure in the innermost few arcmin of the core, centred on the brightest cluster galaxy NGC 4696 (Sanders & Fabian 2002). The iron abundance of the gas was found to peak at a radius of about 1 arcmin from the centre. The temperature drops from 3.5 to about 1 keV over this whole region. A plume-like structure swirls clockwise to the NE beyond which there is an abrupt temperature increase (i.e. a cold front). The central X-ray emission is surrounded by marked dips in emission, or bubbles, which coincide with the complex radio source (Taylor, Fabian & Allen 2002).

Previous X-ray observations (e.g. Allen & Fabian 1994) show a system with smooth, elliptical, X-ray isophotes, indicating the system is relatively relaxed. However, there is evidence for a current or past merger event (Allen & Fabian 1994; Churazov et al. 1999; Furusho et al. 2001; Dupke et al 2001) in the form of shifts in X-ray isophote centroids with radius and bulk motions in the X-ray gas. A neighbouring subcluster, Cen 45 centred on NGC 4709 which is about 15 arcmin E of NGC 4696, has a velocity which is 1500 km s⁻¹ higher than the main Centaurus cluster, Cen 30 (Lucey, Currie & Dickens 1986). Observations of the Centaurus cluster using *ROSAT* and *ASCA* show that the central region of the



Figure 1. Three colour image of the core of the cluster (24 kpc from N to S). Emission between 0.3 and 1 keV is coloured red, 1 to 2 keV green, and 2 to 7 keV blue. The image is 2 m 21 s from N to S which is almost 30 kpc at the distance of NGC 4696.

cluster is particularly rich in metals, with a large abundance gradient (Fukazawa et al. 1994; Ikebe et al. 1998; Allen et al. 2001).

Cluster cores are in detail complex but provide us with an observable analogue of the cooling and heating processes implicit in the formation of massive galaxies. The nearness, intermediate tem-

* E-mail: acf@ast.cam.ac.uk

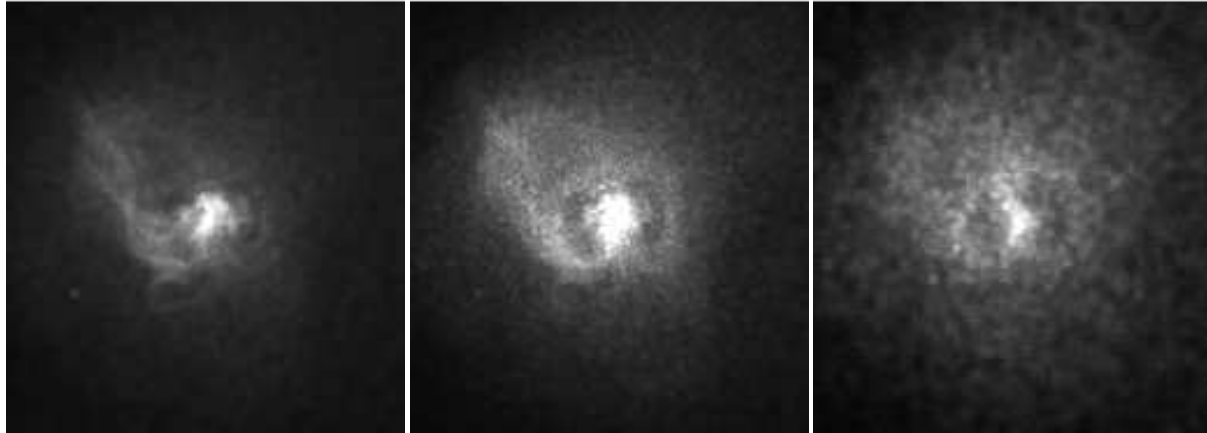


Figure 2. Accumulatively-smoothed images of the core of the cluster in three energy bands. 0.3-1.0 (left), 1.0-2.0 (centre) and 2.0-7.0 (right). The images were smoothed to include a signal to noise ratio of 10 in the smoothing kernel. Each image is 2 m 46 s from N to S.

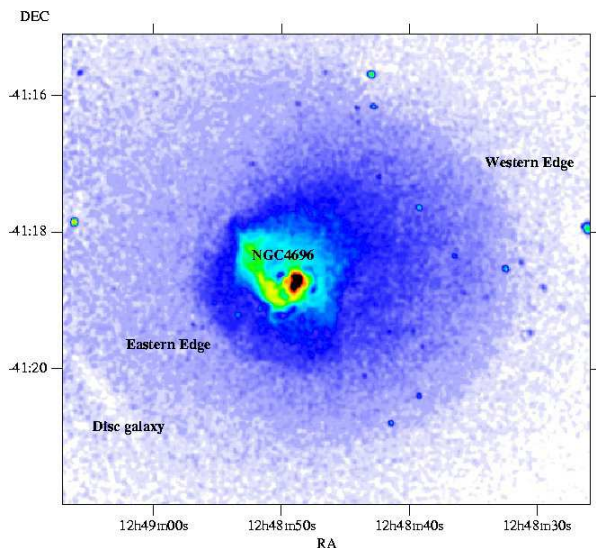


Figure 3. Upper: Detail of the X-ray image in the outer part of the core. The image is in the 0.4 to 7 keV band, smoothed with a Gaussian of ~ 1 arcsec. Using an image smoothed with a Gaussian of ~ 15 arcsec, we subtracted some of the larger scale structure to improve contrast. Various features are marked.

perature, short radiative cooling time and high metallicity make the Centaurus cluster an excellent candidate for studying these processes and also the enrichment of the intracluster gas. Here we present images of the Centaurus cluster from a recent 200 ks *Chandra* observation.

We adopt $H_0 = 70 \text{ km s}^{-1} \text{ Mpc}^{-1}$ which means that one arcsec corresponds to 210 pc at the redshift of the Centaurus cluster.

2 THE DATA

The data presented here are based on *Chandra* OBSIDs 504, 5310, 4954 and 4955. OBSID 504 was first presented in Sanders & Fabian (2002). The standard LC_CLEAN tool was used to remove periods in the observations with possible flares yielding a total good time of 199.3 ks. Each of the datasets were reprocessed to have the latest gain file, and time dependent gain correction was applied. We used

standard blank sky observations to create background spectra for use in spectral fitting.

A 3-band X-ray image of the central core is shown in Fig. 1, with the separate band images in Fig. 2. The images here have been accumulatively smoothed (Sanders et al in preparation; smoothing with a circular top hat kernel with radius determined so that the minimum signal to noise is constant). A whole-band image showing the outer parts is in Fig. 3 and temperature and abundance maps in Fig. 4. The distribution of abundances (scaled to those of Anders & Grevesse 1989) as a function of temperature is shown in Fig. 5. X-ray and optical images of a disc galaxy seen in X-ray absorption are in Fig. 6.

An existing VLA 1.4 GHz image has been overlaid on a whole band X-ray image in Fig 7. The X-ray image has been adaptively-smoothed using an algorithm due to H. Ebeling; features should be significant above the 3-sigma level. New VLA observations were obtained on 2004 October 24 with the VLA in its 'A' configuration. At the observed frequency of 326 MHz this yielded an angular resolution of 17.7×5.6 arcsecond in position angle -4.3 deg. The total time on source was 178 min. The bandwidth used was 12.5 MHz in a 4 IF spectral line mode so as to allow for interference excision using the AIPS task FLGIT. Calibration and imaging of the data were performed in the standard way within AIPS. The final image has an rms noise of 4.8 mJy/beam. This image (Fig. 8, Top) compares well with a 1.4 GHz VLA image previously published (Fig. 7, see also Taylor et al. 2002) and shows that the radio emission extends nearly 2 arcmin (25 kpc) to the south of the nucleus. At the extremities the spectrum is quite steep with a power law index of -1.5 (Fig. 8, Lower).

Strong Faraday Rotation is observed in the central radio source indicating a mean magnetic field of about $8 \mu\text{G}$ at 10 kpc radius (Taylor et al 2002). This corresponds to a magnetic pressure there which is about 2 per cent of the thermal pressure.

3 RESULTS

The longer X-ray exposure has enabled us to see more deeply into the cluster core and resolve much more detail. New features include:

- Filaments extending to the E and NE from the centre are found in the soft X-ray image below 1 keV (Figs. 1 and 2 left). The inner parts of the filaments correspond to the optical filaments and

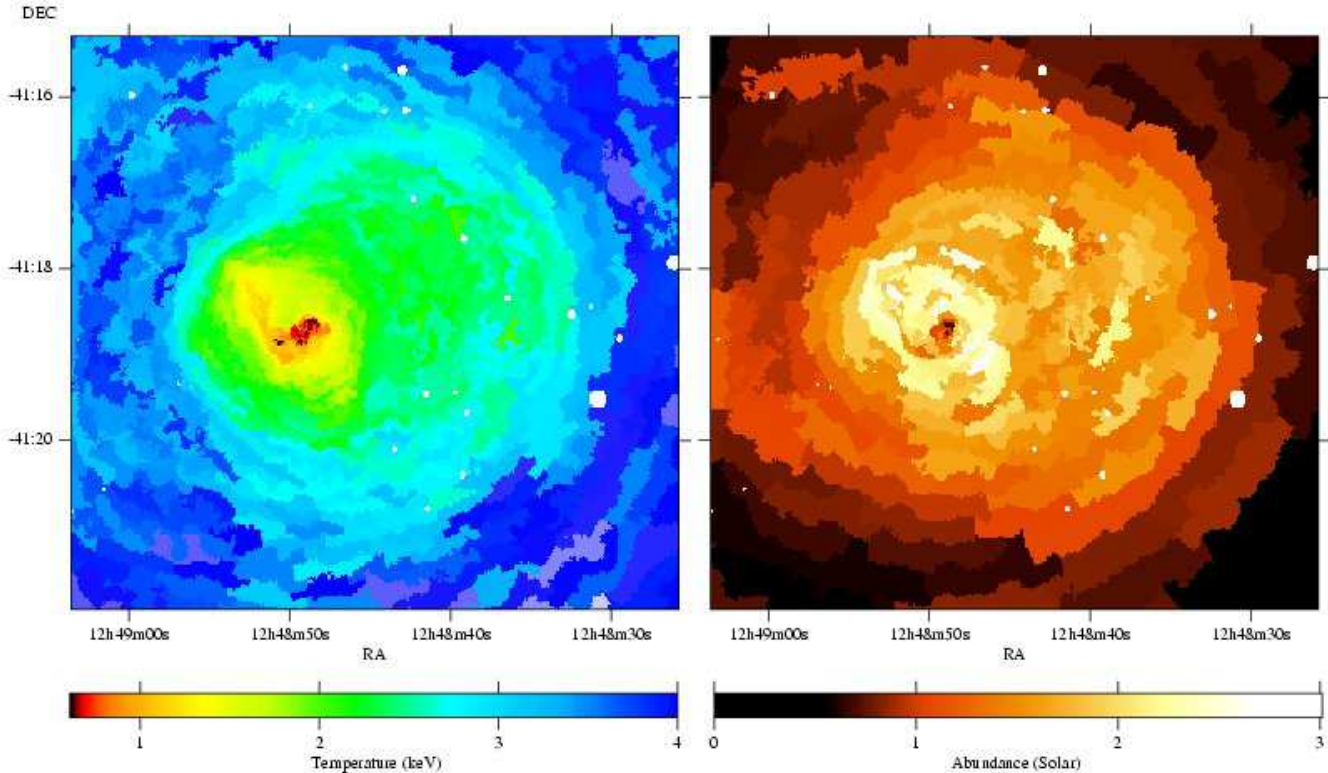


Figure 4. Left: Projected, emission-weighted, temperature map of the cluster. Excluded point sources are marked by white discs. The uncertainties on the temperatures in individual regions containing 2500 counts vary from ~ 0.01 keV in the coolest regions to around 0.5 keV in the hottest regions. Right: Corresponding abundance map measured by fitting spectra in regions containing $\gtrsim 10^4$ counts. Two-temperature models were tested for each region and, where required by an F-test (at better than the 99 per cent level), we have replaced the single temperature abundance by the corresponding two-temperature one. Two temperatures were needed for most of the regions in the temperature map below 2 keV.

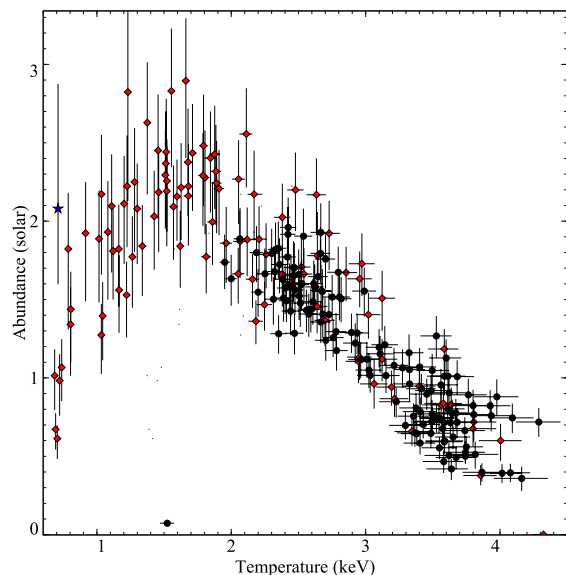


Figure 5. Distribution of abundance as a function of temperature. Abundances obtained from a two-temperature fit are plotted in red using temperatures from the single-temperature fit. The result of using a three-temperature model for the apparent low abundance regions below 0.8 keV is shown by the blue star.

dust lane seen in NGC 4696 (Fabian et al 1982; Sparks, Macchetto

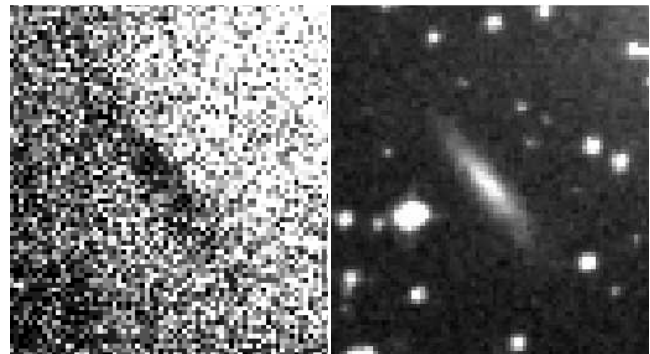


Figure 6. Soft (0.3–0.8 keV) X-ray image (left) of the absorbing disc galaxy seen in the red DSS image (right). Each image is 2.5 arcmin from N to S.

& Golombek 1989). Comparison with new $H\alpha$ images of this region will be presented elsewhere (Crawford et al., in preparation).

- In the 1–2 keV band the holes corresponding to the radio lobes are very clear and above 2 keV the rims of these ‘holes’ or ‘bubbles’ appear bright. The rims do not appear in projection to be hotter (Fig. 4; confirmed by a higher resolution temperature map) and are therefore not shocked. This is similar to results on bubbles found in the Perseus cluster (Fabian et al 2002, 2003). Possible weak ripples in the X-ray surface brightness centred on the nucleus can be seen in Fig. 3, particularly on the NE of the E edge (cf. Fabian et al 2003; Forman et al 2003).

- A loop of gas to the SE (Fig. 2, left) does not coincide with

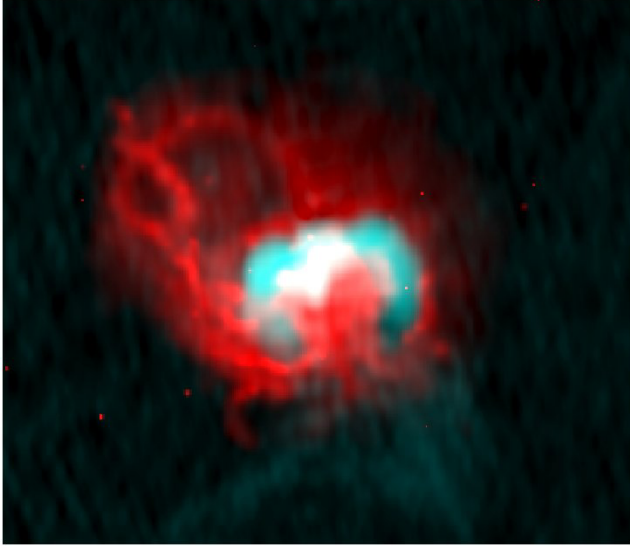


Figure 7. Adaptively-smoothed whole band X-ray image (0.4–7 keV) in red with overlaid 1.4 GHz radio image in blue. The image is 125 arcsec from top to bottom.

any obvious radio structure (Figs. 7 and 8) and could either surround relativistic plasma where the electrons have aged to the extent that they no longer radiate in the observed bands (a ghost bubble), or could just be a loop of cooler X-ray gas. A slight deficit in this region seen in the harder X-ray bands (Figs. 1 and 2) suggests that it is most likely a ghost bubble. A larger loop to the NE appears in the adaptively-smoothed image (Fig. 7). Radio emission is leaking into the inner end (Fig. 8), suggesting that it too is a ghost bubble.

The lop-sided larger scale diffuse emission in the total 0.4–7 keV band was apparent in the earlier image but is now seen much more clearly. It shows a semicircular edge to the E at 83 arcsec (17.5 kpc) from the nucleus (Fig. 3) and a larger semicircular edge to the W at 153 arcsec (32.1 kpc). While the edge to the E is centred on the nucleus of NGC 4696, that to the W is centred 52 arcsec (10.9 kpc) to the W of the nucleus, suggesting that the gas there is in motion with respect to the nucleus.

The edges are clearly evident in the projected temperature map (Fig. 4) and emphasise that the temperature abruptly jumps there by almost 1 keV. They appeared in the radial temperature profiles made from the earlier data (Sanders & Fabian 2002) to both E and W separately. The simplest explanation for them is as cold fronts, such as seen in other clusters (e.g. Markevitch 2000; Vikhlinin et al 2002). Separate deprojection of spectra across the edges to the E and W shows that the pressure across the edges is consistent with being continuous. The abundance drops across both edges; steeply in the case of the W edge (Fig. 4), unlike the cold front in A496 (Dupke & Bregman 2003). The sharp abundance change is similar to behaviour seen in NGC 507 by Kraft et al (2004), although the edge there coincides with a radio lobe, which is not the case here. The large extent of the edges argues against them being simple cold fronts. Sloshing motions of the gas within the central potential well (e.g. Markevitch et al 2001) could account for them and for the E-W asymmetry of the appearance. However, the semicircular shape of the eastern one (see particularly Fig. 3) suggests that this, at least, may have been shaped by disturbances from the nucleus.

The radio source on the other hand appears to be moving to the N, although that may just be an impression from its outer structure

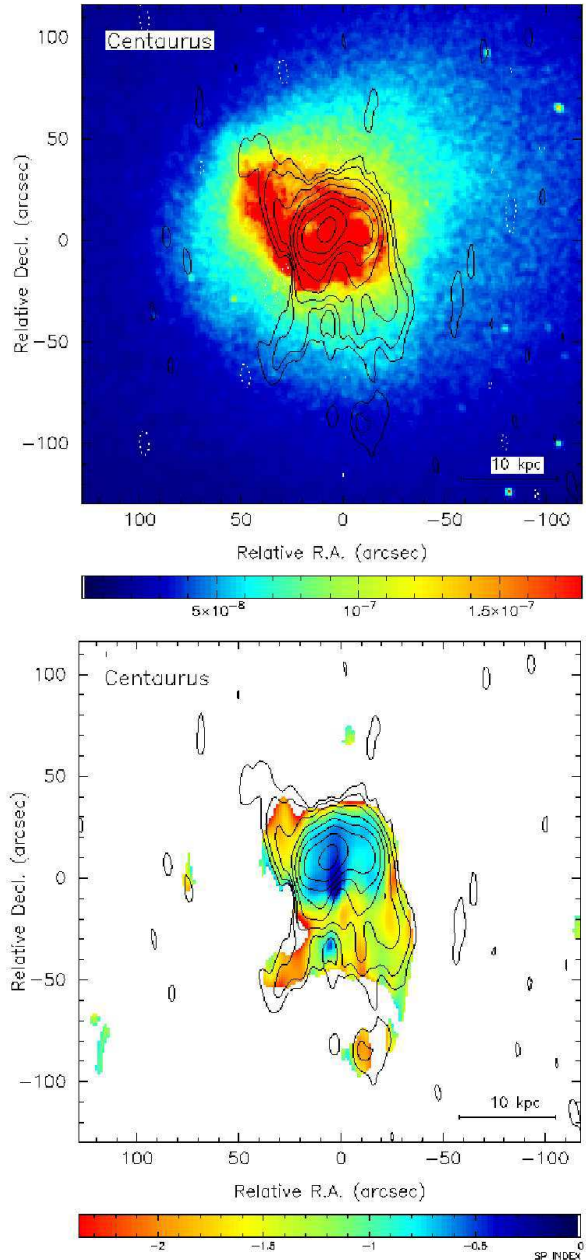


Figure 8. The VLA total intensity image at 330 MHz is shown overlaid on the X-ray image (upper) and on a spectral index map (lower) with contours starting at 20 mJy/beam and increasing by factors of 2. The restoring beam is 17.7×5.6 arcseconds in position angle -4.3 degrees. The radio spectral index (defined $S_\nu \propto \nu^\alpha$) has been computed between 330 and 1565 MHz after convolving the 1565 MHz image to the resolution of the 330 MHz image.

(Fig. 8) which may be following the path of least resistance (the optical image of NGC 4696 shows it significantly flattened in the N-S direction).

The temperature and abundance maps (Fig. 4) reveal that the core of the cluster consists of at least 4 distinct parts. They are a) the region immediately around the nucleus, b) a high abundance region extending 18 kpc to the end of the eastern plume, c) a quasi-spherical region of radius 32 kpc with its centre displaced 11 kpc to the W of the nucleus, and d) the outer region. Each part occupies a

different part of the abundance–temperature plane (Fig. 5) with a) < 1 keV, b) $1 - 2$ keV, c) $2 - 3$ keV and finally d) > 3 keV.

In the present multi-temperature analysis, the abundance peaks at $\sim 2.5 Z_{\odot}$ in b) and drops by about $1 Z_{\odot}$ between b) and c) and c) and d). There cannot be any large turbulent or stochastic motions in the core or these high abundances would have been smoothed out. Following the work of Rebusco et al (2005), who have estimated the diffusion coefficient D in the core of the Perseus cluster, we can obtain a limit from the much higher gradient seen in Centaurus. Assuming stochastic diffusion only, then steep gradients over a distance d are smoothed out on a timescale of d^2/D . If we first look at the outer, western edge and rely only on diffusion to smooth it and adopt a minimum time equal to the local crossing time of the structure of $\sim 5 \times 10^8$ yr then $D < 6 \times 10^{28} \text{ cm}^2 \text{ s}^{-1}$. This is smaller than the result, $D \sim 2 \times 10^{29} \text{ cm}^2 \text{ s}^{-1}$, of Rebusco et al (2005). Since the region is displaced from the central galaxy it is unlikely that any current enrichment has a noticeable effect. Detailed modelling including metal enrichment should yield a tight constraint from the inner, high abundance, region. The above constraint from the outer region means that the level of turbulence and stochastic motions in the Centaurus cluster is low (the product of velocity and lengthscale of the motions being $\sim 3D$). Smallscale motions need continual pumping or they would rapidly die out, temporarily heating the gas, as noted by Rebusco et al (2005).

The lowest energy image reveals delicate filaments of X-ray emitting gas which are only $1-3$ arcsec ($200-600$ pc) wide. The temperature of these structures is about 0.7 keV while the gas they are embedded in has a temperature of about 1.5 keV. Conduction is presumably much reduced and magnetic fields help maintain the integrity of the structures.

In the very core around the nucleus, we can now see that the temperature drops down to less than 0.7 keV, with the inner region being multiphase. The whole temperature range detectable in the Centaurus cluster therefore exceeds a factor of 5, which is significantly larger than the factor of three seen in many other clusters (Peterson et al 2003; but see Morris & Fabian 2004).

A disc galaxy to the SE of NGC 4696 (at RA 12 49 03.8, Dec -41 20 27, J2000.0) can just be seen in silhouette in Fig.3 and, more clearly, in Fig. 6. It has a radial heliocentric velocity of 3737 km s^{-1} (Dickens, Currie & Lucey 1986), so lies in the Cen30 cluster, and is 322-G93 in the ESO/Uppsala catalogue. Photoelectric absorption by galaxies projected onto intracluster gas is also seen in the Perseus (Gillmon et al 2003) and A2029 (Clarke et al 2004) clusters.

4 DISCUSSION

The inner region is complex with radio bubbles, ghost bubbles and cool filaments. The ‘frothy’ X-ray appearance of the centre resembles the centre of the Virgo cluster (Young et al 2002; Forman et al 2003) which also has several inner bubbles. The region beyond is smoother but appears different to the East and West. In those directions clear semicircular edges are seen. The one to the E is concentric with the nucleus indicating that it may have been triggered by a disturbance from there. The larger one to the W is centred west of the nucleus. Its shape suggests that some disturbance from the nucleus may produce it as well.

The Western edge appears as a marked abundance drop, which is not easily accounted for, although large buoyant bubbles dragging iron-rich matter outward, as seen in the Perseus cluster (Sanders, Fabian & Dunn 2004), or fast-moving, outer gas sweep-

ing past as a result of the ongoing merger with Cen 45 (which is not otherwise seen), could contribute.

The dense, metal-rich centre of the Centaurus cluster is revealed as more complex than in previous observations. The radio source clearly has an impact immediately around the centre in the frothy bubble structure and the Eastern edge, although the long-term nature of the interaction and its contribution to the energy balance of the central intracluster medium is elusive. Given that in equilibrium temperature contours follow equipotentials, the asymmetric temperature structure around the central galaxy NGC 4696 means that some major part of the mass or gas distribution there is dynamically changing.

5 ACKNOWLEDGEMENTS

The National Radio Astronomy Observatory is operated by Associated Universities, Inc., under cooperative agreement with the National Science Foundation. GBT acknowledges support for this work from the National Aeronautics and Space Administration through Chandra Award Number GO4-5135X issued by the Chandra X-ray Observatory Center, which is operated by the Smithsonian Astrophysical Observatory for and on behalf of the National Aeronautics Space Administration under contract NAS8-03060. GBT also thanks the Institute of Astronomy for hospitality while working on this project. ACF and SWA thank the Royal Society for support.

REFERENCES

- Allen S.W., Fabian A.C., 1994, MNRAS, 269, 409
 Allen S.W., Fabian A.C., Johnstone R.M., Arnaud K.A., Nulsen P.E.J., 2001, MNRAS, 322, 589
 Anders E., Grevesse N., 1989, Geochimica et Cosmochimica Acta 53, 197
 Churazov E., Gilfanov M., Forman W., Jones C., 1999, ApJ, 520, 105
 Clarke T.E., Blanton E.L., Sarazin C.L., 2004, ApJ, 616, 178
 Dickens R.J., Currie M.J., Lucey J.R., 1986, MNRAS, 220, 679
 Dupke R., Bregman J.N., 2001, ApJ, 562, 266
 Dupke R., White R.E., 2003, ApJ, 583, L13
 Fabian A.C., Nulsen P., Atherton P., Taylor K., 1982, MNRAS, 201, 17P
 Fabian A.C., Celotti A., Blundell K.M., Kassim N.E., Perley R.A., 2002, MNRAS, 331, 369
 Fabian A.C. et al 2003, MNRAS, 344, 43
 Forman W. et al 2003, ApJ, submitted, astro-ph/0312576
 Fukazawa Y., Ohashi T., Fabian A.C., Canizares C.R., Ikebe Y., Makishima K., Mushotzky R.F., Yamashita K., 1994, PASJ, 46, L55
 Furusho T., et al., 2001, PASJ, 53, 421
 Gillmon K., Sanders J.S., Fabian A.C., 2004, MNRAS, 348, 159
 Ikebe Y., Makishima K., Fukazawa Y., Tamura T., Xu H., Ohashi T., Matsushita K., 1999, ApJ, 525, 58
 Kraft R.P., et al 2004, ApJ, 601, 221
 Lucey J.R., Currie M.J., Dickens R.J., 1986, MNRAS, 221, 453
 Markevitch M., et al 2000, ApJ, 541, 542
 Markevitch M., Vikhlinin A., Mazzotta P., 2001, ApJ, 562, L153
 Morris R.G., Fabian A.C., 2004, MNRAS submitted (astro-ph)
 Peterson, J.R., et al 2003, ApJ, 590, 207
 Rebusco P., Churazov E., Böhringer H., Forman W., 2005, MNRAS submitted, astro-ph/0501141
 Sanders J.S., Fabian A.C., 2002, MNRAS, 331, 273
 Sanders J.S., Fabian A.C., Dunn R.J.H., 2004, MNRAS, submitted
 Sparks W., Macchetto F., Golombek D., 1989, ApJ, 345, 153
 Taylor G.B., Fabian A.C., Allen S.W., 2002, MNRAS, 334, 769
 Vikhlinin A., Markevitch M., Murray S.S., 2001, ApJ, 551, 160
 Young A.J., Wilson A.S., Mundell C.G., 2002, ApJ, 579, 560